Refereed Proceedings

The 12th International Conference on Fluidization - New Horizons in Fluidization Engineering

Engineering Conferences International *Year* 2007

Bubble Size and Mass Transfer in a Modified Airlift Loop Reactor with Continuous Slurry Phase

Mengxi Liu* Chunxi Lu†

Mingxian Shi‡

*Chinese University of Petroleum (Beijing), mengxiliu@sina.com

†Chinese University of Petroleum (Beijing), lcxing@cup.edu.cn

‡Chinese University of Petroleum (Beijing)

BUBBLE SIZE AND MASS TRANSFER IN A MODIFIED AIRLIFT LOOP REACTOR WITH CONTINUOUS SLURRY PHASE

Liu Mengxi, Lu Chunxi, Shi Mingxian,
The State Key Laboratory of Heavy Oil Processing
Faculty of Chemical Engineering, China University of Petroleum Beijing
18 Fuxue Road, Changping, Beijing, China, 102249
T: 0-8610-89733803; F: 0-8610-89733803; E: mengxiliu@sina.com

ABSTRACT

A modified internal airlift loop reactor with continuous slurry phases was explored to investigate the local bubble size and the local mass transfer properties. A mathematical model was derived to simulate the bubble size in every flow region. Also, a new method was developed to measure the dissolved oxygen concentration.

INSTRUCTION

In order to meet different industrial processes, many types of modified gas-liquid-solid hybrid reactors have emerged in recent years. In this study, an experimental apparatus was employed as a cold model of a novel hybrid reactor designed for hydrate formation, F-T and methanol syntheses, and so on. As an important base of optimization and scale-up of the hybrid reactor, the local hydrodynamics and local mass transfer property was investigated. The hybrid reactor mainly includes three parts: spray-impinge part, perforated plate part, and modified internal airlift loop reactor (MIALR) part. The focus was mainly placed on the MIALR part.

Most literatures published were addressed on the internal airlift loop reactor (IALR) operated with batch operation of liquid or slurry. This quite limits extended application of the IALR in processes such as hydrate formation and F-T, in which the solid product must be entrained by liquid and discharged continuously. In this study, some modifications were made on an IALR in order to operate with continuous operation of slurry. As the feed tube of slurry, a downcomer tube was located with a distance of 290mm above the gas distribution. A 50 mm ID pipe was mounted at the conical bottom of MIALR for discharging. In order to avoid mixing of gas circulated from annulus with feed gas from distributor, and to avoid entrainment of gas by discharged slurry, the bottom of the MIALR was specially designed to be a conical section. The distance of L_1 was intentionally selected in order to provide a bigger flow area than that of annulus (see Fig.1), which dramatically slows the velocity of circulation slurry from annulus. Therefore, most bubbles move back to annulus and only few bubbles can be entrained into the draft tube. Moreover, the specially designed conical bottom has a relatively big space, which leads to a long residence time of slurry, and thereby most bubbles in the discharge slurry are degassed.

Owing to complexity of multi-phase flow and limitation of measurement techniques,

The 12th International Conference on Fluidization - New Horizons in Fluidization Engineering, Art. 38 [2007]

studies on local hydrodynamics and local mass transfer properties in IALR has been rare, although the lack of these information quite limits the optimum and the commercialization of IALR. The present study addressed the distribution of bubble size and local mass transfer properties of MIALR.

EXPERIMENTAL

A schematic diagram of the experimental apparatus is shown in Fig. 1. The MIALR is made of Plexiglas with 284 mm in inner diameter and 1700 mm in height. A draft tube, 186mm in inner diameter and 1000mm in height, is situated coaxially inside the MIALR, and the ratio of the cross-sectional area of the draft tube to that of annulus is 0.85. In order to feed and discharge slurry continuously, two 50 mm ID pipes are mounted coaxially inside the draft tube and the bottom of MIALR, respectively. The bottom of the MIALR is a conical section with a cone angle of 60°. Water and air were used as the liquid and gas in the experiments. The solid is high density polyethylene (HDPE) particle, with a density and mean diameter of 881.6 kg·m^3 and 243μm, respectively. In order to be hydrophilic, polyvinyl chloride was employed for pretreatment. The superficial velocity of slurry, U_{Lr}, and the superficial gas velocity, U_{Gr}, varies from 0.03 to 0.05m·s^{-1} and 0.006 to 0.19 m·s^{-1}, respectively, based on the cross-sectional area of draft tube. The solid loading is from 5% to 15%.

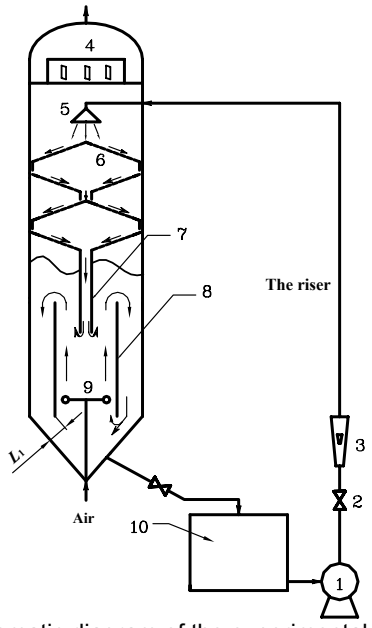

Fig. 1 Schematic diagram of the experimental apparatus
1. pump, 2. valve, 3. rotameter, 4. gas-liquid separator, 5.spray, 6. perforated plate, 7. downcomer tube, 8. draft tube, 9. ring distributor, 10. tank

The local bubble size was measured by using a dual-electrode resistance probe. Details of the measuring method and data processing were described elsewhere (Lo (7)). All chord length distributions of bubbles are found to follow a modified log-normal distribution given below, in which δ, ξ and γ are parameters of equation.

$$P_c(l_b) = \frac{\delta}{\sqrt{2\pi}\cdot\xi\cdot l_b}\exp\left[-\frac{(\ln l_b-\gamma)^2}{2\xi^2}\right] \quad (1)$$

In the classical air/N_2 steady-state method to estimate the k_La, the difference of the inlet and outlet slurry of hybrid reactor is about 8 or 9 mg/L. The small difference

leads to big error for the hybrid reactor employed. There are three parts in the hybrid reactor, in which the spray-impinge part is proved to have extremely high $k_L a$ over the other two. As a result, the difference of oxygen concentration between the inlet and outlet of MIALR is no more than 3 mg/L, which leads to a smaller difference of oxygen concentration between different axial positions, and thereby brings to big measurement error. Therefore, a new steady-state method was developed. As shown in Fig.1, the liquid is supersaturated by stripping with pure oxygen in a tank and then pumped into the hybrid reactor. When the supersaturated liquid contacts with air, the dissolved oxygen transfers to air. In this method, the difference of the dissolved oxygen concentration of the inlet and outlet liquid is as high as 14 mg/L, which reduces the measurement error dramatically. The dissolved oxygen concentration is measured with a covered membrane galvanic oxygen sensor (WTW Model Cellox325) with the dynamic response time less than 5s. In order to determine the saturated solubility of oxygen in water, liquid temperatures are also measured.

RESULTS AND DISCUSSION

Flow regions

The flow of gas and slurry is diversified and complicated in the ALR. Verlaan (11) revealed that the flow of gas and slurry is near plug-flow in draft tube and annulus, and well-mixed in gas-liquid separation region. Merchuk (9) found $k_L a$ is different in draft tube, annulus and separation region. Also, he found that IALR can be divided into three flow regions, draft tube, annulus and gas-liquid separator. However, in MIALR, more regions should be taken into account, which do affect the hydrodynamics and mass transfer performance significantly. For instance, gas distributor region contributes much to mass transfer performance. Actually, the contact efficiency of gas and liquid in this region is higher efficient than that in most regions. Furthermore, bottom of IALR is another region which should be considered. Although few bubbles are in this region, the design of the bottom region does considerably influent the magnitude of circulating bubbles, and suspension of particles (Luan (8)). For MIALR, there is a special region, downcomer affected region (see Fig. 1), which ranges from the exit of the downcomer tube to the top of the gas distributor region. According to the experimental data of this study, the hydrodynamic and the mass transfer characteristics in the downcomer affected region is quite different with that in other regions. Therefore, there are six flow regions in the MIALR: the gas distributor region, the downcomer affected region, the draft tube region, the gas-slurry separation region, the annulus region and the bottom region. Specially, the definition of the draft tube region here is different with that in literatures. In this study, the draft tube region is the zone from the upper end of the draft tube to the exit of the downcomer tube. More details about the six flow regions are shown in Fig. 2.

Local and overall bubble sizes

Fig.3 shows the axial variation of the cross-sectional average bubble size ($\bar{d}_b$) in the draft tube. It is seen that with h/D_c less than 0.43, corresponding to the region from the gas distributor to the bottom of the draft tube, $\bar{d}_b$ is less than 3mm, which is dramatically smaller than that in other regions of MIALR. It is due to the fact that the special conic bottom supplies a sharply extended flow channel, and the bubbly slurry from the annulus is dramatically slowed. Therefore, only few small bubbles are entrained into the draft tube. This behavior signifies that the cross-sectional area of flow channel for bottom can prevent or promote the circulation of bubbles from the

The 12th International Conference on Fluidization - New Horizons in Fluidization Engineering, Art. 38 [2007]

annulus to the draft tube. With h/D_c beyond 0.43 and up to 1.08, corresponding to the gas distributor and downcomer affected regions, $\bar{d}_b$ increases substantially along the axial position. When h/D_c is above 1.08, $\bar{d}_b$ increases progressively until the h/D_c of 2.09 is reached. Beyond this h/D_c, in the gas-slurry separation region $\bar{d}_b$ increases rapidly again with the increase of h/D_c. Similar phenomena are also found in other literature. Lo (7) reported that $\bar{d}_b$ became larger for the top of the draft tube and the separation region. The evolution of $\bar{d}_b$ in the annulus region along the axial position is shown in Fig.4. It can be seen that the change of $\bar{d}_b$ is small, implying an equilibrium of coalescence and breakage of bubbles. Moreover, $\bar{d}_b$ in the annulus region is evidently smaller than that observed in other regions except bottom region.

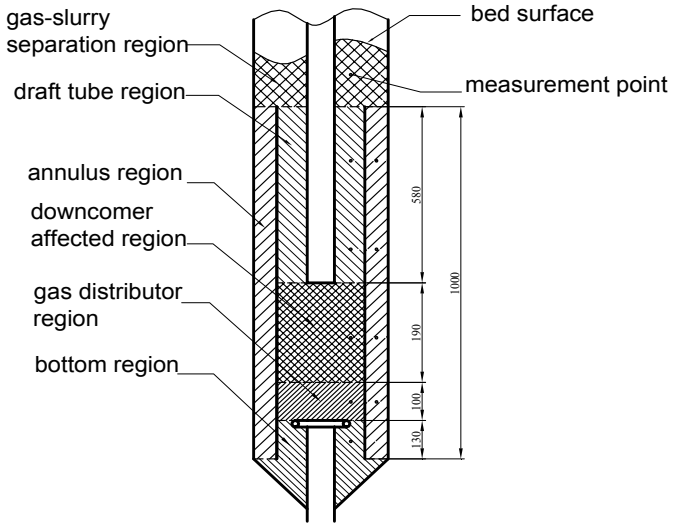

Fig. 2 Sketch of flow regions and axial measurement positions

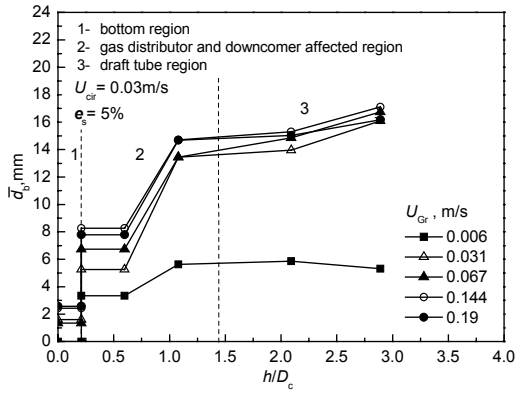

Fig.3 The axial variation of cross-sectional average bubble size in the draft tube

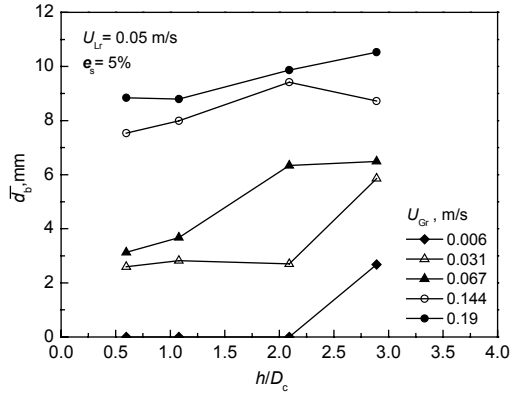

Fig.4 The axial variation of cross-sectional average bubble size in the annulus

During the motion of single bubbles, they are not only deformed but also break up, and the condition for breakup bubbles can be written as:

$$\frac{\rho_G u_{gl}^{\ 2}}{2} = \frac{3\sigma_h^{\ 3}}{r_b^{\ 3}\rho_h^{\ 2}u_{gl}^{\ 4}} \qquad (2)$$

Levich (6) reported that large-scale eddies have no influence on the bubbles, so that the deformation and breakup of a bubble is caused by comparatively small turbulent eddies whose characteristic velocity can be written as (David (2)):

$$U_e \simeq (\epsilon \lambda)^{1/3} \tag{3}$$

where ϵ is the energy dissipation and λ the scale of eddies capable of breaking up the bubbles. This scale is approximately that of critical bubble diameter, so that $\lambda \simeq 2r_b$. Furthermore, the relative velocity of the bubble is approximately same as the eddy velocity, $U_{gl} \simeq U_e$ (David (2)).

The energy dissipation, ϵ, can be expressed as the following equation (Frisch (4)):

$$\epsilon \simeq k \cdot U^3 / l \tag{4}$$

where k is a constant. U and l are the characteristic velocity and the characteristic size of the large-scale eddies, respectively, and defined as (David (2)):

$$l = h_j / (1 - \bar{\varepsilon}_T) \tag{5}$$

$$U = const \cdot (g h_j)^{1/2} \tag{6}$$

where $\bar{\varepsilon}_T$ is the mean gas holdup of the fluidized bed. Substitution of equations (3), (4), (5), (6) into equation (2) leads to:

$$d_b = 2r_b = g_1 \left(\frac{\sigma_h}{\rho_h g A} \right)^{3/5} (1 - \bar{\varepsilon}_T)^{-2/5} \left(\frac{h_j}{D} \right)^{-1/5} \left(\frac{\rho_h}{\rho_G} \right)^{1/5} \tag{7}$$

where A and D are the cross-sectional area and the diameter of the fluidized bed. Eq. (7) is the mathematical model of the critical bubble size. However, in the MIALR employed in this study, the effects of bubble coalescence, the solid loading and the superficial slurry velocity are not negligible. Therefore, the equation factors $\bar{\varepsilon}_T^{\,h_5}$, $\left(\frac{\varepsilon_s}{\varepsilon_{s0}} \right)^{h_4}$ and $\mathrm{Re}_{Lr}^{\,h_2}$ should be introduced, and the Eq.(7) can be rewritten as

$$\bar{d}_T = h_8 \mathrm{Re}_{Lr}^{\,h_2} \left(\frac{1}{1 - \bar{\varepsilon}_T} \right)^{3/5} \left(\frac{\varepsilon_s}{\varepsilon_{s0}} \right)^{h_4} \left(\frac{\sigma_h}{\rho_h g A} \right)^{3/5} \left(\frac{\rho_h}{\rho_G} \right)^{1/5} \left(\frac{H}{D} \right)^{-1/5} \bar{\varepsilon}_T^{\,h_5} \tag{8}$$

where H is the height of fluidized bed. Obviously, Eq.(8) is suitable for any flow regions of MIALR. In each flow region, the equation factor H/D can be taken to be a constant and the variation of $\frac{\sigma_h}{\rho_h g A_z}$ and $\frac{\rho_h}{\rho_G}$ is small enough to be neglected. On simplifying, the mean bubble diameter in flow regions can be written as

$$\bar{d}_{z,T} = h_1 \mathrm{Re}_{Lr}^{\,h_2} \left(\frac{\bar{\varepsilon}_{z,T}}{1 - \bar{\varepsilon}_{z,T}} \right)^{h_3} \left(\frac{\varepsilon_s}{\varepsilon_{s0}} \right)^{h_4} \tag{9}$$

The mean bubble size in six flow regions are simulated and calculated by Eq.9. The results are shown in Table1 with errors less than 20%.

Table 1 Values of model parameter in Eq. 9

Flow regions	h_1	h_2	h_3	h_4
The bottom region	6.09	-0.088	0.154	-0.176
The gas distributor region	7.16	-0.005	0.3	-0.417
The downcomer affected region	36.76	-0.208	0.338	-0.591
The draft tube region	65.2	-0.226	0.378	-0.45
The gas-slurry separation region	44.62	-0.201	0.43	-0.46
The annulus region	98.60	-0.142	0.775	-0.118

The 12th International Conference on Fluidization - New Horizons in Fluidization Engineering, Art. 38 [2007]

Local and overall volumetric gas-liquid mass transfer coefficients

In gas-liquid-solid fluidization bed, many models were used to estimate gas-liquid mass transfer coefficient, k_La, by fitting the axial oxygen concentration distribution in the liquid at steady state. For instance, the backflow cell model (BFCM), the plug flow model (PFM) and the axial dispersion model (ADM). Although these models have been used to predict mass transfer property of conventional fluidization bed successfully, they might result in big error for calculating k_La in more complicated fluidization bed with different flow patterns. In IALR, the flow mode in different region has been proved to be quite different (Merchuk (9)), which results in different k_La in different regions. Therefore, the ideal solution to this problem would be to employ different models for different regions. In present work, the MIALR is modeled by employing six ideal regions as shown in Fig.2. The CSTR model is used for the gas distributor region, the downcomer affected region and the gas-slurry separation region. The CSTR model is expressed as

$$k_L a = \frac{Q}{V}\frac{(C_{in} - C)}{C - C*} \tag{10}$$

The ADM model is used for draft tube region and annulus region. According to axial dispersion model, the oxygen mass balance in liquid phase can be written as

$$\frac{1}{Pe_L}\frac{d^2C}{dx^2} - \frac{dC}{dx} + St_L(C - C^*) = 0 \tag{11}$$

where C^* can be expressed as

$$C^* = y(a - bx) \tag{12}$$

The Eq.11 is complemented with the following boundary conditions:

$$\begin{cases} x = 0, \quad C = C_0, \quad y = y_0 \\ x = 1, \quad \left[dC/dx \right]_{x=1} = 0 \end{cases} \tag{13}$$

Due to the low solubility of oxygen in water, the change of oxygen concentration in the gas phase is extremely small and neglected. The above Eq. 11 and 14 can be solved analytically or numerically. Pe_L is calculated by Han (5)

$$Pe_L = 3.2 \times 10^{-4}\,\mathrm{Re}_L\,\mathrm{Re}_G^{-0.5}\left(1-\varepsilon_s\right)^{2.8} \tag{14}$$

The gas-liquid mass transfer coefficient is obtained by parameter fitting of solution of equations to the experimentally determined dissolved oxygen concentration profile. The comparison of oxygen concentration distribution in the draft tube region fitted by model to that experimentally measured is shown in Fig.5. It is seen that because the hight of the draft tube is small, the curve of resolved oxygen concentration is near line. The error of Fig.5 is less than 5%.

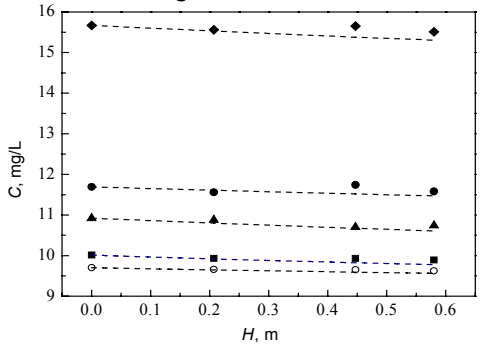

Fig.5 Comparison of oxygen concentration distribution fitted by model to experimental data

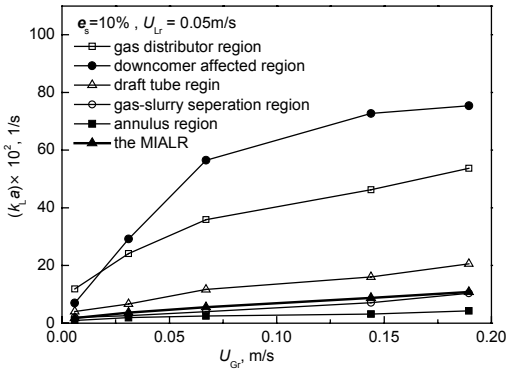

Fig.6 Comparison of k_La for different regions and the whole reactor

Fig.6 shows k_La for different regions and the whole reactor. Comparison shows a substantial difference for k_La. The k_La is notably large for the gas distributor and downcomer affected region. As shown in Fig.1, the feed slurry is introduced directly into the draft tube, which leads to the descending feed slurry impinges with ascending bubbly slurry. Therefore, the turbulence of bubbly slurry dramatically enhanced, and the coalescence of bubbles is impeded. As a result, the size of bubbles decreases, and the interfacial area *a* increases. It is seen in Fig.6 that mass transfer of oxygen to gas mainly occurred in the draft tube, thus, the increase of the ratio of the volume of the draft tube, especially of the volume of the downcomer affected region, to that of whole MIALR is helpful to reinforce the mass transfer capability of MIALR. Moreover, the k_La for the whole reactor, $(k_La)_{MIALR}$, is close to that for the gas-slurry separation region, and the k_La for the annulus region is very small. According to experimental data, the difference between oxygen concentration of inlet and outlet of the bottom region is approximately equal, thus it is accepted that there is no mass transfer occurred in the bottom region.

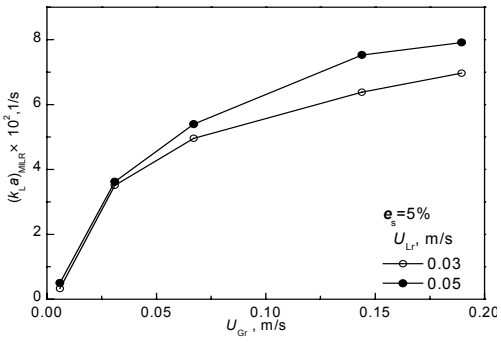

Fig.7 Effect of gas velocity on $(k_La)_{MIALR}$ as a function of slurry velocity

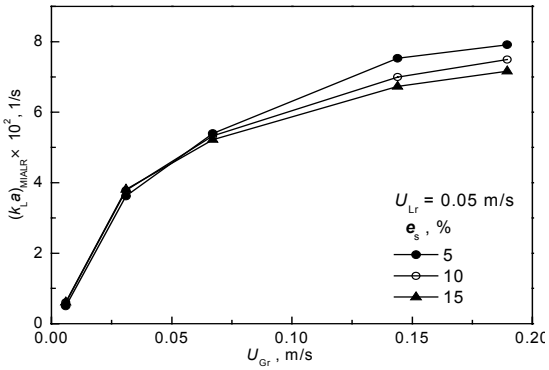

Fig.8 Effect of gas velocity on $(k_La)_{MIALR}$ as a function of solid loading

Figs.7 and 8 show the effects of the superficial gas velocity on k_La, as the function of superficial slurry velocity and solid loading, respectively. It is seen that k_La increases with an increase in superficial gas velocity. The evolution of $(k_La)_{MIALR}$ is familiar to that obtained by Contreras (1), which shows a sharp increase when U_{Gr} is small and slow increase when U_{Gr} is large. However, the transition point of the curve for both experiments is different. As shown in Fig.7 and 8, the transition velocity is 0.067m/s, while Contreras (1) found this velocity is 0.05m/s. He also revealed that the range of U_{Gr} less than 0.05m/s corresponds to the uniform bubbly flow. This means that the MIALR has a wider operating range for the uniform bubbly flow. Also, it is found that $(k_La)_{MIALR}$ in this study is higher than that obtained in conventional IALR with respect to gas-liquid system (Contreras (1)) and gas-liquid-solid system (Freitas (3)).This behavior might arise from the fact that to introduce the feed slurry into the draft tube enforces the turbulence of slurry, and thereby decreases bubble size, which leads to a higher k_La for MIALR. It is also seen that k_La increases with an increase in the superficial slurry velocity, whilst decreases with the increase of solid loading. This is because the increase of superficial slurry velocity and solid loading result in the decrease of bubble size, and therefore *a* increases.

CONCLUSIONS

Experiments were conducted to investigate the local bubble size distribution and

gas-liquid mass transfer characteristics of a modified IALR with slurry as a continuous phase. The bubble size is found to increase with the increase of the superficial gas velocity. A mathematical model is driven for simulating the mean bubble size in the six flow regions. A new method was developed to measure the dissolved oxygen concentration in liquid. It is found that the volumetric gas-liquid mass-transfer coefficient increases with increasing the superficial velocities of gas and slurry, whilst decreases slightly with increasing the solid loading.

ACKNOWLEGEMENTS

This work is financially supported by National Key Basic Research Project (973) of the People's Republic of China under grant No. 2005CB221205, and by National Natural Science Foundation of China under grant No. 20676147.

NOTATION

C^*	Equilibrium concentration of oxygen, mg/L
D_L	Axial dispersion coefficient, m^2/s
Pe	Peclet number
St	Stanton number

REFERENCES

1 Contreras, A., Gracía, F., Molina, E., Merchuk, J.C., Influence of sparger on energy dissipation, shear rate, and mass transfer to sea water in a concentration-tube airlift bioreactor. *Enzyme and Mocrobial Technology*, 1999, **25**, 820-830

2 David, A., Two-phase flows in chemical engineering. UK: Cambridge Univ. Press, Cambridge, 1981.

3 Freitas, C., Teixeira, J.A., Oxygen mass transfer in a high solids loading three-phase internal-loop airlift reactor. *Chem. Eng. Sci*., 2001, **84**, 57-61

4 Frisch, U., Turbulence. UK: Cambridge Univ. Press, Cambridge, 1995

5 Han, S.J., Zhou, J., Jin, Y., Wang, Z., Phase holdup and liquid distribution in gas-liquid- solid circulating fluidized bed. *Chin. J. Chem. Eng.*, 1997, *5*, 246.

6 Levich, V.G., Physicochemical hydrodynamics. Englewood Cliffs, NJ: Prentice-Hall, 1962.

7 Lo, C.S., Hwang, S.J., Local hydrodynamic properties of gas phase in an internal-loop airlift reactor. *Chem. Eng. J*., 2003, **91**, 3~22

8 Luan, M.F., Mao, Z.S., Wang, R., Chen, J.Y., Effects of bottom configuration and circulation direction of gas-lift loop on solid suspension. *Eng. Chem. Metal*., (China), 1994, **15,** 260-264.

9 Merchuk, J.C., Osemberg, G, Siegel, M, A method for evaluation of mass transfer coefficient in the different regions of airlift reactors. *Chem. Eng. Sci*., 1992, **47**(9~11): 2221~2226

10 Miyahara, T., Kawate, O., Hydrodynamics of a solid-suspended bubble column with a draft tube containing low-density particles. *Chem. Eng. Sci*., 1993, **48**, 127~133

11 Verlaan, P., Tramper, J., Van't Riet, K., A hydrodynamic model for an airlift-loop bioreactor with external loop. *Chem. Eng. J*., 1986, **33**, B43-B53.